CHEMCONFLUX[20] Special Issue

J. Indian Chem. Soc.,
Vol. 97, No. 10a, October 2020, pp. 1694-1698

Heat energy storage using parabolic dish collector in $LiNO_3$ phase change material

B. Kumar*[a], M. K. Das[b] and J. N. Roy[a]

[a]School of Energy Science and Engineering, [b]Department of Mechanical Engineering,

Indian Institute of Technology Kharagpur, Kharagpur-721 302, West Bengal, India

E-mail: brajeshkumar998@gmail.com

Manuscript received online 10 July 2020, revised and accepted 14 October 2020

A detailed investigation of heat energy storage using parabolic dish collector in $LiNO_3$ phase change material (PCM) has been presented here. In this study, we investigate the energy storage capacity of PCM for different mass fractions. 3-D enthalpy based numerical model is used for this investigation. Constant heat flux for 1 kW system simulation is used for the bottom surface of the container for 6 hours per day. We observed that the total energy stored by all mass of PCM is equal in the 4th hour. After complete melting of PCM energy storage capacity reduces. Therefore, depending upon the utility, we should select the PCM.

Keywords: Heat flux, numerical model, parabolic dish collector, phase change material, thermal energy storage.

Introduction

Solar energy has the potential to meet the energy requirements of domestic and industrial processes, but there is a time mismatch between solar energy supply and energy demand by the process. In this case, thermal energy storage allows the use of solar energy without the presence of solar radiation. Among the different ways of energy storage, latent heat thermal energy storage[1], i.e. phase change material (PCM), is very attractive. There are many PCM available for thermal applications but among all the PCM, $LiNO_3$ is medium temperature range PCM having cost-effective, and good heat storage capacity. Therefore $LiNO_3$ is an interesting area of the present work. Work done on PCM heat storage by multiple authors is listed in Table 1.

Application of solar thermal energy with the industrial process will eliminate CO_2 emissions and fossil fuel consumptions. However, the industry has problems to use solar energy due to ample space requirement, but PCM can resolve this issue and can supply heat energy at a constant rate for different thermal applications in the industry and households.

Table 1. Work was done on latent heat storage by various authors

Methods	Reference
1D Enthalpy	2–5
1D and 2D Enthalpy	6, 7
2D Enthalpy	8–10
Experimental	11–13

Numerical study

The heat transfers in container and PCM are assumed to be transient and three-dimensional. Body forces and convection are neglected. The container and PCM interface are uniform. Purely conductive and radiative heat transfer is allowed for all domains. For modelling, a three-dimensional heat transfer 3-D enthalpy based model has been used. Enthalpy based model is the best model for the study of the phase-field model. Many authors have used enthalpy based model in 1-D or 2-D. In this work, the 3-D model is used, all three dimensions are considered for simulation. It gives more accuracy, but its cost of simulation is very high. The governing equations are:

$$\rho\frac{\partial H}{\partial t} - k\nabla^2 T = \ddot{Q} \quad (1)$$

For solid container

$$H = c_p T \quad (2)$$

For solid-phase PCM

$$H = c_p T : (T \leq T_m - \varepsilon) \quad (3)$$

For transition phase PCM

$$H = c_p T + \frac{\lambda}{2\varepsilon}(T - T_m + \varepsilon) : (T_m - \varepsilon \leq T \leq T_m + \varepsilon) \quad (4)$$

For liquid phase PCM

$$H = c_p T + \lambda : (T \geq T_m + \varepsilon) \quad (5)$$

Nondimensional Stefan number (*Ste*)

$$Ste = \frac{c_p (T_m - \varepsilon - T_b)}{\lambda} \quad (6)$$

Melt fraction (ϕ)

$$\phi = (1 - Ste) \quad (7)$$

Effective thermophysical property during the transition phase

$$\rho_e = \phi\rho_s + (1 - \phi)\,\rho_l : (T_m - \varepsilon \leq T \leq T_m + \varepsilon) \quad (8)$$

$$k_e = \phi k_s + (1 - \phi)\,k_l : (T_m - \varepsilon \leq T \leq T_m + \varepsilon) \quad (9)$$

$$C_{pe} = \frac{1}{\rho_e}\left(\phi\rho_s c_{ps} + (1 - \phi)\,\rho_l c_{pl}\right) + \lambda\frac{\partial\alpha_m}{\partial T} \quad (10)$$

$$\alpha_m = \frac{1}{2}\frac{(1 - \phi)\,\rho_l - \phi\rho_s}{\phi\rho_s + (1 - \phi)\,\rho_l} \quad (11)$$

where c_p (kJ/kg-K) is specific heat capacity, H (kJ/kg) is enthalpy, k (W/m-K) is thermal conductivity, $\ddot{Q}$ (W/m^3) is volumetric heat generation, T_b (K) is bulk temperature of PCM, T_m (K) is melting temperature, α_m is the amount of the PCM which is under melting process, *Ste* is Stefan number, ε (K) is transition interval between solid to the liquid phase[14], ϕ is solid-phase PCM, λ (kJ/kg) is the heat of fusion, subscripts *s* for solid-phase PCM and *l* liquid phase PCM.

Simulation, validation and grid independent test

3-D enthalpy based model is computed using COMSOL 5.3a Multiphysics®. The simulation domain and grid generation are shown in Fig. 1 and Fig. 2. Various assumptions have been taken for the simulation setup. (1) The solid container and PCM interface is uniform. (2) The solid-liquid interface of PCM is progressed uniformly. (3) Transport properties of the solid-liquid phases of the PCM are negligible. (4) Superheating and subcooling effects are neglected. (5)

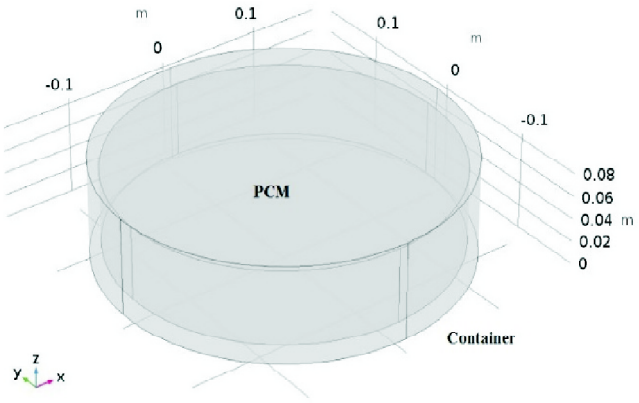

Fig. 1. Simulation domain of container and PCM.

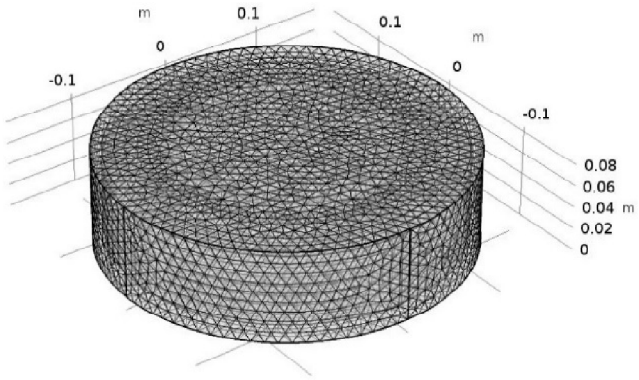

Fig. 2. Grid generation of container and PCM.

The Backward Differentiation Formula (BDF) and Parallel Sparse Direct Solver PARADISO is used for numerical simulation.

Three different sets of grids are generated using the mesh generation module. First set of grids 44004, the second set of grids 88106 and third set of grids 176012 are taken for simulation. Grid independence test of temperature vs time shown in Fig. 3. Grid set of 88106 and 176012 show identical temperature vs time distribution at the centre of the PCM. Therefore an optimal set of grid 88106 is used for further computation.

The present computational model is validated with Zivkovic and Fujii[2] and Siyabi *et al.*[15]. Temperature variation vs time shows good agreement of the present simulation setup with the published benchmark which is shown in Fig. 4 and Fig. 5.

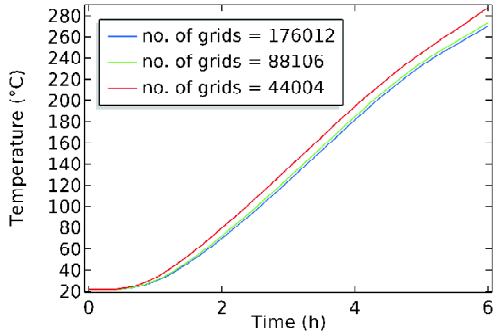

Fig. 3. Grid independence test of present work concerning temperature vs time at the centre of the PCM.

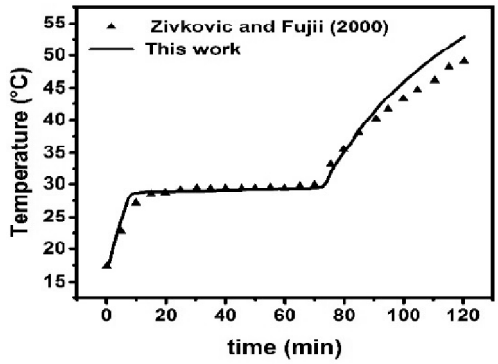

Fig. 4. Validation of this work with Zivkovic and Fujii[2].

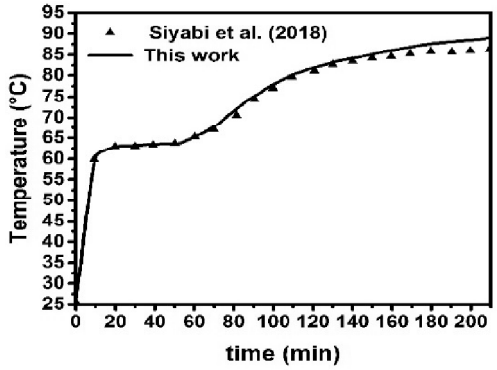

Fig. 5. Validation of this work with Siyabi *et al.*[15].

Results and discussion

Stainless steel polished container[14], the outer radius of 16.7 cm, the height of 16.2 cm, and thickness 10 mm is filled with a different mass of phase change material (PCM) $LiNO_3$. Mass of the PCM is selected based on receiver volumetric capacity and density of PCM. The mass of PCM filled in the container is 23.8 kg, 21.4 kg, 16.7 kg, and 11.9 kg (10%, 30% and 50% mass reduction respectively). Radially variable constant inward heat flux is taken for the bottom surface, and all surface is exposed at a constant surface emissivity of 0.1 for radiation heat transfer. Heat flux on the receiver surface is shown in Table 2.

Initial and boundary condition

When $t \leq 0$

$T(\bar{s}, 0) = T_i = 295$ K

when $t > 0$ heat flux at the receiver surface is given in Table 2.

Table 2. Heat flux variation in the radial direction at the bottom surface (taken from ray optics simulation for 1 kW solar parabolic dish collector system for six hours a day on receiver surface)

R (m)	Heat flux (kW/m^2)	R (m)	Heat flux (kW/m^2)
0.003	78.70	0.097	55.74
0.026	73.38	0.115	49.65
0.048	68.36	0.138	44.03
0.067	63.34	0.154	35.96
0.087	58.63	0.166	18.02

The total energy stored by the PCM is shown in Table 3.

Table 3. Total energy stored by PCM vs time

Time (h)	Total energy (kJ) of the different mass (kg) of PCM			
	23.8	21.4	16.7	11.9
1	3765	3662	3628	3589
2	8955	8710	8728	8322
3	14115	13828	13426	13059
4	19201	18878	18792	18587
5	24312	23368	22962	21754
6	29161	27312	26408	23981

Comparison of enthalpy vs temperature, melt fraction vs time, total stored energy vs time, and bulk temperature vs time of different mass of $LiNO_3$ is shown in Figs. 6–9 respectively. Melting starts after half-an-hour, and after 4th h 11.9 kg of $LiNO_3$ gets completely melted, but 16.7 kg, 21.4 kg, and 23.8 kg of $LiNO_3$ get 75%, 55%, and 48% melted after 4th h. Energy stored by 23.8 kg of PCM is 21.6% more than the energy stored by 11.9 kg of $LiNO_3$ after the 6th h.

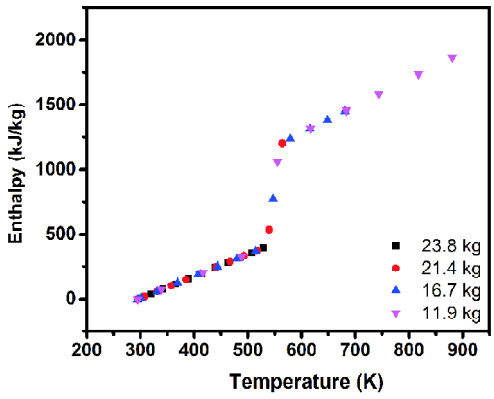

Fig. 6. Comparison of enthalpy vs temperature for the different mass of $LiNO_3$.

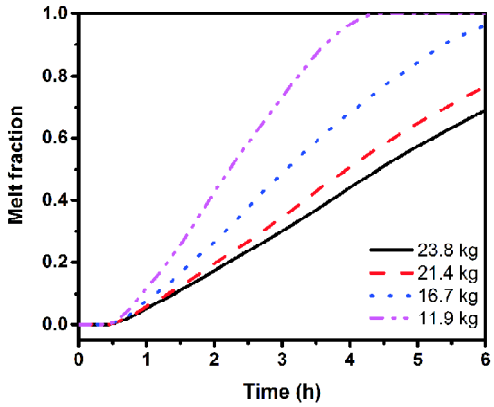

Fig. 7. Comparison of melt fraction vs time for the different mass of $LiNO_3$.

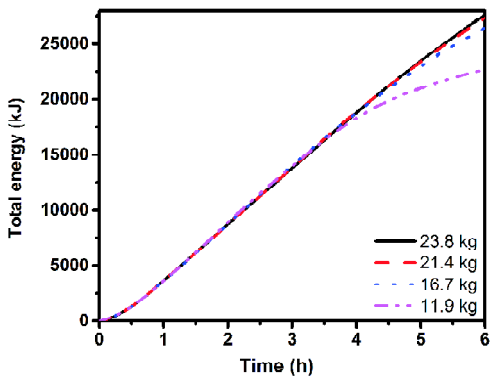

Fig. 8. Comparison of stored energy vs time for the different mass of $LiNO_3$.

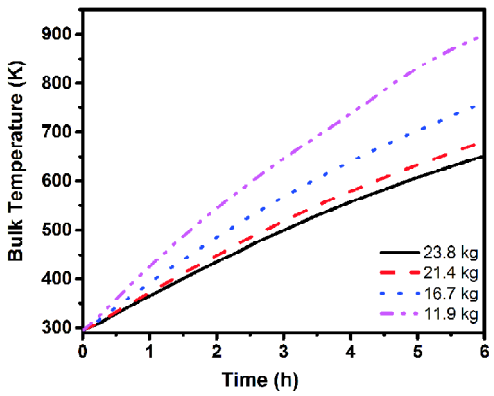

Fig. 9. Comparison of bulk temperature vs time for the different mass of $LiNO_3$.

Conclusions

The bulk temperature of 11.9 kg of $LiNO_3$ is higher than the 23.8 kg of $LiNO_3$ PCM. The total energy stored by 11.9 kg of $LiNO_3$ is less at the end of 6th h. Total energy sored by all mass of PCM is approximately equal in the 4^{th} hour because after complete melting of PCM energy storage capacity reduces. Energy stored by 23.8 kg of PCM is 21.6% more than the energy stored by 11.9 kg of $LiNO_3$. After complete melting of PCM sensible heating factor becoming a dominating factor over latent heating.

Integrating the storage with discharge using heat application, after 4th h, 11.9 kg of $LiNO_3$ is more efficient than the 23.8 kg of $LiNO_3$ because storage cost is almost half, but stored energy is almost same.

References

1. F. Javadi, H. Metselaar and P. Ganesan, *Sol. Energy*, 2020, **206**, 330.
2. B. Zivkovic and I. Fujii, *Sol. Energy*, 2001, **70**, 51.
3. A. D. Solomon, *Sol. Energy*, 1979, **22**, 251.
4. D. Lecomte and D. Mayer, *Appl. Energy*, 1985, **21**, 55.
5. P. D. Silva, L.C. Gonçalves and L. Pires, *Appl. Energy*, 2002, **73**, 83.
6. M. Costa and A. Oliva, *Interface*, 1998, **39**, 319.
7. R. Velraj, R. V. Seeniraj, B. Hafner, C. Faber and K. Schwarzer, *Sol. Energy*, 1999, **65**, 171.
8. D. Li, Y. Ding, P. Wang, S. Wang, H. Yao, J. Wang and Y. Huang, *Energies*, 2019, **12**, 1.
9. M. Esen, A. Durmş and A. Durmş, Geometric design of solar-aided latent heat store depending on various parameters and phase change materials, *Sol. Energy*, 1998, **62**, 19.

10. K. A. R. Ismail and M. M. Abugderah, *Energy Convers. Manag*., 2000, **41**, 1165.
11. J. C. Choi and S. D. Kim, *Energy*, 1992, **17**, 1153.
12. A. Sarý and K. Kaygusuz, *Energy Convers. Manag*., 2002, **43**, 2493.
13. A. Hasan, *Sol. Energy*, 1994, **52**, 143.
14. G. A. Lane, "Solar Heat Storage: Latent Heat Materials", Vol. II, CRC Press, Taylor & Francis Group, 2018.
15. I. Al Siyabi, S. Khanna, T. Mallick and S. Sundaram, *Energies*, 2018, **11**, 2.